Theory of gas–gas phase transition in raregas binary mixtures

Lidia Strigari, Mauro Rovere, and Bruno D'Aguanno

Citation: The Journal of Chemical Physics **105**, 2020 (1996); doi: 10.1063/1.472070
View online: http://dx.doi.org/10.1063/1.472070
View Table of Contents: http://scitation.aip.org/content/aip/journal/jcp/105/5?ver=pdfcov
Published by the AIP Publishing

Theory of gas–gas phase transition in rare-gas binary mixtures

Lidia Strigari and Mauro Rovere
Dipartimento di Fisica, Università della Calabria, INFM, Unità di Cosenza, 87036 Arcavacata di Rende, Italy

Bruno D'Aguanno[a)]
CRS4, Centro di Ricerca, Sviluppo e Studi Superiori in Sardegna, Via N. Sauro, 10, 09123 Cagliari, Italy

(Received 18 January 1996; accepted 10 April 1996)

The lines of critical points of rare-gas binary mixtures are evaluated within the framework of a statistical mechanics theory of thermodynamic stability, recently developed by Chen and Forstmann. The phase instabilities are related to the local compositional and density order in the fluid through a density functional expansion of the grand canonical potential. The structural inputs are determined by using the thermodynamically self-consistent integral equation scheme known as hypernetted chain/mean spherical approximation (HMSA). A good agreement is obtained with neutron scattering data of He–Xe and Ne–Xe mixtures near the phase transition. Although the accuracy in reproducing the experimental critical point lines is only semi-quantitative, the qualitative behaviors are properly described. For the first time, a detailed microscopic interpretation of the so called behavior of the ''second type'' of the critical line is given. © *1996 American Institute of Physics.* [S0021-9606(96)50927-X]

I. INTRODUCTION

The immiscibility of gases, or gas–gas equilibrium, was predicted more than 100 years ago by van der Waals,[1] and it was experimentally confirmed, for the first time, by Krichevskii *et al.* in 1940, and by Tsiklis in 1952, who studied, respectively, N_2–NH_3 and He–NH_3 systems (see Schneider[2] and references therein). Since then, the progress of high pressure techniques made it possible to investigate the gas–gas equilibria in a number of different binary mixtures.[2,3] This immiscibility phenomenon also became extremely important for chemical engineering applications.[4]

Two main types of gas–gas critical behaviors were observed, and classified according to the shape of the line of the critical points (CPL) in the pressure versus temperature plane. In gas–gas equilibria, the CPL always starts from the critical point of the less volatile component. The ''first type'' behavior is defined by a monotonous increase of the pressure as the temperature is increased. In the ''second type'' behavior, the CPL is characterized by an initial decrease of the temperature, with a positive or negative slope, by a minimum in the temperature value, and by a final increase of the pressure as the temperature starts again to increase. The point of the CPL corresponding to the minimum in temperature is called double critical point (DCP).

These phenomena are of great interest for what concerns the long standing problem of connecting microscopic interaction forces to the phase diagrams of fluids. Although it is well established that rare gas can be successfully described through simple models, like the Lennard-Jones potential, a complete microscopic theory of the phase transition is still missing.[5,6] Only phenomenological theories, which have been proposed for a long time,[2,3,7] and few computer simulation results[8–10] are available.

Very recent progress in the statistical mechanics description of the stability limits of multicomponent thermodynamic systems give the possibility of improving the understanding of gas–gas equilibria, thus motivating this present work. We are referring to the hierarchical reference theory of Parola and Reatto,[6] which goes beyond the mean field approximation, and to the theory based on density functional of Chen and Forstmann.[11] In both approaches one can predict the different fluctuations which contribute to the mechanical and material instabilities at the spinodal transition point. In this paper we apply the Chen and Forstmann approach to reconstruct the CPL of He–Xe and Ne–Xe mixtures at high pressure. Our interest in these systems also comes from the availability of neutron scattering data[12,13] on the microscopic structure near phase transition for both mixtures. Another source of interest is the different critical behavior shown by the two type of mixtures: He–Xe mixtures have a CPL of the first type, while Ne–Xe a CPL of the second type.

To locate the CPL, in both the (T,P) and (x,P) planes, we used the following procedure. The fluid structure is determined through the use of the Zerah and Hansen closure,[14] called HMSA, by assuming a Lennard-Jones potential for the particle–particle interaction (at this stage, comparisons with neutron scattering data are performed). The solution of HMSA, which provides all the correlation functions of interest, is then used in the density functional expansion of the grand canonical potential. By diagonalizing this expansion, the smallest eigenvalue, which corresponds to the softest mode, is found and the spinodal line is located. By changing the macroscopic parameters of the investigated system, the sketched procedure is repeated a number of times until all the CPL is reconstructed.

We chose this localization procedure since it allows the determination of both the particular kind of phase transition mechanism, which is established when the stability limit is by-passed, and the composition of the new formed phases.

[a)]Author to whom correspondence should be addressed.

 0021-9606/96/105(5)/2020/8/$10.00

We note that such predictions cannot be achieved by simpler approaches, such as those based on the van der Waals equation.[7]

A localization of the critical points via interpolation of the binodal branches of the immiscibility region, which often gives more accurate results,[15] is also possible. However, since the calculation of the binodal lines is based on the integration of the pressure and on the internal energy along given thermodynamic paths, is not infrequent to reach states for which integral equations do not provide a solution, making the method useless.

The paper is organized as follows. We first review the thermodynamic stability conditions of multicomponent systems, and relate them to the Bhatia–Thornton structure factors. Then, it is shown how such structure factors enter in the Chen and Forstmann expansion of the grand canonical potential, and how it is possible to locate the limit of stability from an analysis of the diverging fluctuations. In Sec. III, applications of the HMSA to mixtures of He–Xe and Ne–Xe are presented, and comparisons with experimentally determined structure factors are made. Section IV summarizes all the steps of the procedure to locate the spinodal lines and the line of critical points. Such lines are shown in Sec. V, where detailed discussions of all predictions of the outlined working scheme are presented. Finally, Sec. VI is dedicated to the summary and conclusions.

II. THERMODYNAMICS AND STATISTICAL MECHANICS OF INSTABILITY

It is well known that infinitesimal local fluctuations of thermodynamic properties are always present in equilibrium states, and that if such fluctuations are dumped by the reaction of the system itself (Le Chatelier's principle), then the equilibrium states are also stable states. When instead by changing the thermodynamic state of the system some fluctuations are amplified, the system becomes locally unstable and phase transitions are observed which, in turn, restore a new equilibrium stable situation (this is also a manifestation of the Le Chatelier's principle). By using the notation of Callen,[16] the conditions which express the local stability of thermodynamic equilibrium states of a system with M components are

$$u[P_0,P_1,\ldots,P_j]_{jj}=\left(\frac{\partial P_j}{\partial y_j}\right)_{P_0,P_1,\ldots,P_{j-1},y_{j+1},\ldots,y_{M-1}} >0 \quad \text{for all } j=0,1,\ldots,M. \tag{1}$$

In this expression, the quantities P_j are the intensive variables of the differential form of the fundamental equation of thermodynamics

$$u=u(S/N,V/N,N_1/N,N_2/N,\ldots,N_M/N) =u(y_0,y_1,y_2,\ldots,y_{M-1}) \tag{2}$$

in which the extensive quantities have been rescaled by the total number of particles N.

For a two-component system at constant N, the stability conditions become

$$\left(\frac{\partial P_0}{\partial y_0}\right)_{v,y_2}=\left(\frac{\partial T}{\partial s}\right)_{v,x_1}=\frac{T}{c_v}>0, \tag{3}$$

$$\left(\frac{\partial P_1}{\partial y_1}\right)_{T,y_2}=-\left(\frac{\partial P}{\partial v}\right)_{T,x_1}=\frac{1}{v\kappa_T}>0, \tag{4}$$

$$\left(\frac{\partial P_2}{\partial y_2}\right)_{T,P}=\left(\frac{\partial(\mu_1-\mu_2)}{\partial x_1}\right)_{T,P}=\left(\frac{\partial^2 g}{\partial x_1^2}\right)_{T,P}>0, \tag{5}$$

where c_v is the specific heat at constant volume, κ_T is the isothermal compressibility, g is the molar Gibbs free energy, and $y_2=N_1/N=x_1$, is the molar fraction of component 1.

The first condition (thermal stability) tells us that the temperature must increase when heat is applied to the system; the second (mechanical stability) tells us that the pressure must decrease when the system is isothermically expanded; while the third (material stability) tells us that energy must increase when a particle is added to the system. If one of these conditions is violated, the system looses its stability and reacts making a phase transition, which could be a fluid–fluid or/and a mixing–demixing transition, a fluid–solid transition or a solid–solid transition. Here, we are interested in studying fluid–fluid and mixing–demixing transitions which are induced by the loss of mechanical and material stabilities.

To build a statistical mechanics theory of instability it is necessary to (i) link the previous expressions to fluctuations of given microscopic quantities, and (ii) to derive expressions which allow the clear identification of the transition mechanism. Step (i) has been accomplished, by Kirkwood and Buff[17] and by Bhatia and Thornton.[18] Recently, their approach has been reviewed and generalized to fluid mixtures of any number of components by Gazzillo.[19,20] Step (ii) has been established by Chen and Forstmann[11] and by Parola and Reatto.[6]

By following the work of Bhatia and Thornton,[18] the isothermal compressibility, κ_T, and the second derivative of the Gibbs free energy, $(\partial^2 g)/(\partial x_1^2)_{T,P}$, are linked to the long wavelength limit of the correlations between the total number density and composition fluctuations through the exact relations

$$S_{NN}(k)=\frac{1}{N}\langle \delta n_k^N \delta n_{-k}^N\rangle \overset{k=0}{\rightarrow} nk_BT\kappa_T+\Delta^2 k_BT \Big/ \left(\frac{\partial^2 g}{\partial x_1^2}\right)_{T,P}, \tag{6}$$

$$S_{NC}(k)=\frac{1}{N}\langle \delta n_k^N \delta n_{-k}^C\rangle \overset{k=0}{\rightarrow} -x_1x_2\Delta k_BT \Big/ \left(\frac{\partial^2 g}{\partial x_1^2}\right)_{T,P}, \tag{7}$$

$$S_{CC}(k)=\frac{1}{N}\langle \delta n_k^C \delta n_{-k}^C\rangle \overset{k=0}{\rightarrow} (x_1x_2)^{1/2}k_BT \Big/ \left(\frac{\partial^2 g}{\partial x_1^2}\right)_{T,P}, \tag{8}$$

where the $\delta n_k^{N,C}$ are the Fourier components of the total number fluctuations, $\delta n^N(r)$, and of the compositions fluctuations, $\delta n^C(r)$, defined as

$$\delta n^N(r)=\delta n_1(r)+\delta n_2(r), \tag{9}$$

$$\delta n^C(r) = (1-x_1)\,\delta n_1(r) - x_1\,\delta n_2(r). \tag{10}$$

In addition, n is the total number density and Δ is the dilatation factor given by

$$\Delta = n(\overline{v_1} - \overline{v_2}) = -\frac{1}{n}\left(\frac{\partial n}{\partial x_1}\right)_{T,P,N}, \tag{11}$$

with $\overline{v_1}$ and $\overline{v_2}$ the partial molar volumes of the two species.

The collection of points in which stability is lost, namely, the spinodal line, is then identified by divergences in the $k=0$ limit of the Bhatia–Thornton structure factors $S_{NN}(k)$, $S_{NC}(k)$, and $S_{CC}(k)$.

To locate the spinodal line in the thermodynamic state diagram, and to identify to what extent the related transition is of the condensation/evaporation (C/E) or mixing/demixing (M/D) type, Chen and Forstmann[11] made a functional expansion of the grand free energy of the system, $\Omega(T,V,\mu_\alpha;[n_\alpha])$, around the equilibrium densities n_α ($\alpha=1,2$). By truncating the expansion at the second order term, they obtained a relation between the variation of Ω and a correlation matrix, $\mathbf{M}(k)$, whose elements are linked to the Bhatia–Thornton structure factors and, via the Kirkwood and Buff relations, to the stability conditions. This last link identifies $\mathbf{M}(k=0)$ as the thermodynamic stability matrix. The relation is

$$\delta\Omega(\mathbf{M}(k)) = \frac{k_B T}{2V}\sum_k \left[\lambda_1(k)\left|\delta\overline{n}_1(k)\right|^2 + \lambda_2(k)\left|\delta\overline{n}_2(k)\right|^2\right], \tag{12}$$

where the fluctuation terms $\delta\overline{n}_{1,2}(k)$ are defined by

$$\delta\overline{n}_i(k) = X_{i,1}(k)\,n^{-1/2}\delta n^N(k) + X_{i,2}(k) \times (n/x_1x_2)^{1/2}\delta n^C(k). \tag{13}$$

In this equation, the vector $\mathbf{X}_i(k)$ is the eigenvector which diagonalize the matrix $\mathbf{M}(k)$, whose associated eigenvalues $\lambda_{1,2}(k)$ are given by

$$\lambda_{1,2}(k) = (M_{NN}(k) + M_{CC}(k) \mp \sqrt{(M_{NN}(k)-M_{CC}(k))^2 + 4M_{NC}(k)})/2, \tag{14}$$

while the elements of the matrix $\mathbf{M}(k)$ are defined through the Bhatia–Thornton structure factors as follows:

$$S_{NN}(k) = \mathbf{M}^{-1}_{NN}(k), \tag{15}$$

$$S_{NC}(k) = x_1x_2\mathbf{M}^{-1}_{NC}(k), \tag{16}$$

$$S_{CC}(k) = (x_1x_2)^{1/2}\mathbf{M}^{-1}_{CC}(k). \tag{17}$$

At the spinodal line, one of the eigenvalues $\lambda_{1,2}(k)$ goes to zero, and the corresponding eigenvector defines the precise combination of fluctuations, δn^N and δn^C [see Eq. (13)], which are diverging.

The only part which is still missing in this statistical mechanics approach to instability is a theory to evaluate the Bhatia–Thornton structure factors. To this purpose, we chose, from the integral equation theory, the thermodynamically self-consistent hypernetted mean spherical approximation (HMSA) scheme, originally developed by Zerah and Hansen.[14]

This scheme consists of the Ornstein–Zernike equations

$$h_{\alpha\beta}(r) = c_{\alpha\beta}(r) + n\sum_\lambda x_\lambda \int d\mathbf{r}'\, h_{\alpha\lambda}(r)c_{\lambda\beta}(|\mathbf{r}-\mathbf{r}'|), \tag{18}$$

which are exact relations, together with the HMSA closures

$$h_{\alpha\beta}(r) = -1 + \exp[-\beta v^{\mathrm{rep}}_{\alpha\beta}(r)] \times\left(1 + \frac{\exp(f(r)[h_{\alpha\beta}(r) - c_{\alpha\beta}(r) - \beta v^{\mathrm{att}}_{\alpha\beta}(r)]) - 1}{f(r)}\right). \tag{19}$$

Once the repulsive, $v^{\mathrm{rep}}_{\alpha\beta}(r)$, and the attractive, $v^{\mathrm{att}}_{\alpha\beta}(r)$, part of the particle–particle interaction potential are given, the HMSA scheme is a ''closed'' set of equations which can be numerically solved. The solution is achieved by enforcing thermodynamic consistency, that is, the equality between the isothermal compressibilities obtained from the fluctuation and the virial route.[14,21] The identity to be satisfied can be written as

$$4\pi n\int_0^\infty dr\, r^2 \sum_{\alpha\beta} x_\alpha x_\beta c_{\alpha\beta}(r) = \frac{\partial}{\partial n}\left[\frac{2\pi n^2\beta}{3}\int_0^\infty dr\; r^3 \sum_{\alpha\beta} x_\alpha x_\beta \frac{dv_{\alpha\beta}(r)}{dr}\, g_{\alpha\beta}(r)\right], \tag{20}$$

and the equality of the two terms is reached by systematically changing the parameter ξ which appears in the mixing function, $f(r)$, defined as

$$f(r) = 1 - \exp(-\xi r). \tag{21}$$

The ''results'' of the HMSA scheme are the direct correlation functions $c_{\alpha\beta}(r)$ and the total correlation functions $h_{\alpha\beta}(r) = g_{\alpha\beta}(r) - 1$, where $g_{\alpha\beta}(r)$ are the pair distribution functions.

By Fourier transforming the set of $h_{\alpha\beta}(r)$ functions, the needed Bhatia–Thornton structure factors of the two-component system of interest are obtained from the relations

$$S_{NN}(k) = 1 + n[x_1^2\widetilde{h}_{11}(k) + x_2^2\widetilde{h}_{22}(k) + 2x_1x_2\widetilde{h}_{12}(k)], \tag{22}$$

$$S_{NC}(k) = nx_1x_2[x_1\widetilde{h}_{11}(k) - x_2\widetilde{h}_{22}(k) + (x_2-x_1)\widetilde{h}_{12}(k)], \tag{23}$$

$$S_{CC}(k) = 1 + nx_1x_2[\widetilde{h}_{11}(k) + \widetilde{h}_{22}(k) - 2\widetilde{h}_{12}(k)]. \tag{24}$$

The full location of the spinodal line is, at this point, straightforward.

TABLE I. Lennard-Jones interaction parameters.

	Xe–Xe[a] Set 1	Xe–Xe[b] Set 2	Ne–Ne[a]	He–He[b]	Ne–Xe[c] Set 1	Ne–Xe[c] Set 2	He–Xe[c] Set 1	He–Xe[c] Set 2
$\epsilon_{\alpha\beta}/k_B$ (K)	222.3	230	35.6	10.2	88.96	90.49	47.62	48.44
$\sigma_{\alpha\beta}$ (Å)	4.1	3.85	2.75	2.56	3.425	3.3	3.33	3.205

[a]Values from Ref. 7.
[b]Values from Ref. 12.
[c]Values obtained from the Lorentz–Berthelot rule [see Eq. (27)].

III. ONE-PHASE MICROSCOPIC STRUCTURE

Before proceeding to the full application of the localization framework outlined in the previous section, it is important to check if the proposed integral equation scheme, namely, the HMSA, is accurate in describing the microscopic structure of the binary mixtures under investigation. To this purpose, we applied the HMSA scheme to the He–Xe and Ne–Xe mixtures experimentally studied, respectively, by Bellisent-Funel *et al.*,[12] and by Filabozzi *et al.*[13]

In their work, Bellisent-Funel *et al.*[12] reported neutron scattering data for the total structure factor, $S^t(k)$, of two thermodynamic states of the He–Xe mixture close to the demixing surface. Such structure factor is given by

$$S^t(k)=1+\frac{1}{(x_1\bar{b}_1+x_2\bar{b}_2)^2}\,(\bar{b}_1^2 S_{11}(k)+\bar{b}_2^2 S_{22}(k) +2\bar{b}_1\bar{b}_2 S_{12}(k)), \tag{25}$$

where the coefficients b_α are the coherent scattering length of the two species, and the partial structure factors, $S_{\alpha\beta}(k)$, are the Fourier transform of the pair distribution functions $g_{\alpha\beta}(r)$

$$S_{\alpha\beta}(k)=x_\alpha\delta_{\alpha\beta}+nx_\alpha x_\beta\int d\mathbf{r}\; e^{-i\mathbf{k}\cdot\mathbf{r}} g_{\alpha\beta}(r). \tag{26}$$

From these definitions, it is evident that the total structure factor, $S^t(k)$, can be theoretically evaluated by solving the set of Eqs. (18), (19), and (20), once the appropriate microscopic parameters characterizing the two species are supplied.

The Lennard-Jones interaction parameters of the pure elements He, Ne, and Xe are reported in Table I, together with the crossed interaction parameters as obtained from the Lorentz–Berthelot (LB) rule

$$\epsilon_{12}^{\mathrm{LB}}=\sqrt{\epsilon_{11}\epsilon_{22}}, \qquad \sigma_{12}^{\mathrm{LB}}=(\sigma_{11}+\sigma_{22})/2. \tag{27}$$

The values of coherent scattering lengths b_α are taken from standard nuclear data tables.

By defining the attractive and repulsive part of the Lennard-Jones potential

$$v_{\alpha\beta}(r)=4\epsilon_{\alpha\beta}\left(\left(\frac{\sigma_{\alpha\beta}}{r}\right)^{12}-\left(\frac{\sigma_{\alpha\beta}}{r}\right)^{6}\right), \tag{28}$$

according to the Weeks, Chandler, and Andersen prescription,[22] we solved the HMSA scheme by using a rapidly convergent Picard procedure introduced by Ng.[23]

Figure 1 shows a comparison between the experimental data and the HMSA results for the two He–Xe mixtures of Ref. 12. A quantitative agreement is obtained, although the mixtures are very close to the transition line, as it is evident from the extremely high value of $S^t(k)$ at $k=0$.

Analogous results for a Ne–Xe mixture are shown in Fig. 2. Since more than one set of Lennard-Jones interaction parameters are reported in the literature we performed two different calculations according to the parameters labeled set 1 and set 2 of Table I. It is observed that the best agreement is obtained for set 2 [Fig. 2(b)], which corresponds to a smaller value of the Xe diameter. However, more extended tests of the HMSA accuracy, and of the validity of the LB rule could not be performed, due to the fact that experimen-

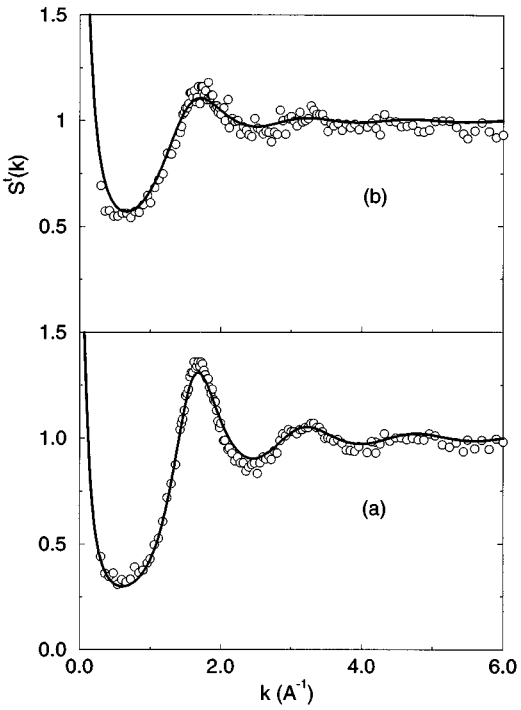

FIG. 1. Total structure factor of two He–Xe mixtures. Circles: experimental data from Ref. 12; Lines: HMSA results. Parameters of (a): $T=294.6$ K, $x_{\mathrm{Xe}}=0.78$, $n=9.49\times10^{21}$ atoms/cm^3; Parameters of (b): $T=294.6$ K, $x_{\mathrm{Xe}}=0.48$, $n=7.08\times10^{21}$ atoms/cm^3. Other input quantities are from set 2 of Table I.

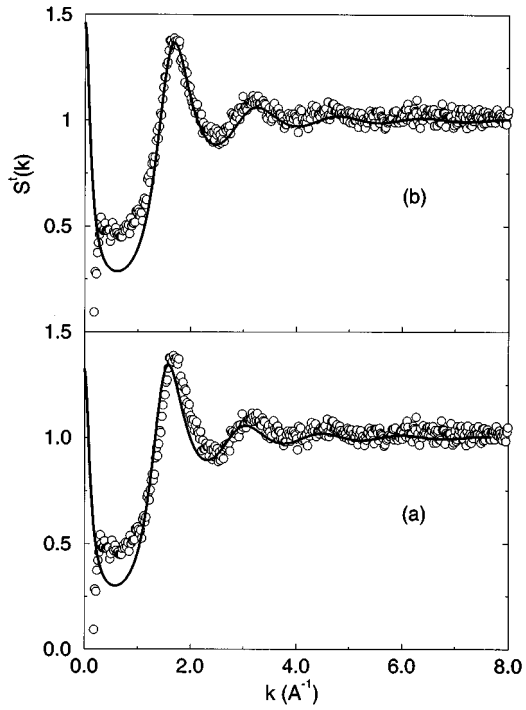

FIG. 2. Total structure factor of a Ne–Xe mixture. Circles: experimental data from Ref. 13; Lines: HMSA results. In (a), the HMSA results are obtained by using parameter set 1 of Table I, while in (b) has been used set 2. Other parameters are $T=275$ K, $x_{\mathrm{Xe}}=0.81$, $n=7.9\times10^{21}$ atoms/cm^3.

tally measured partial structure factors, $S_{\alpha\beta}(k)$ are not available.

IV. LOCALIZATION OF SPINODAL LINES AND CRITICAL POINTS

To locate the spinodal line of a binary mixture it is necessary to fix the density of the mixture, and to change both the composition and the temperature until vanishing eigenvalues of the diagonalization procedure of Sec. II are found. By repeating such a procedure for different densities, it is then possible to reconstruct the full line of critical points.

More specifically, we proceeded in the following way. We started from a region where the system is homogeneous and, for a given density, composition, temperature, and interaction parameters, we solved the HMSA equations. We then decreased the temperature, while keeping constant the density and the composition. At this point, we evaluated the eigenvalues, λ_1 and λ_2, and we followed the one which approaches zero. Getting closer to the instability region, it becomes more difficult to find thermodynamically self-consistent solutions of HMSA, and to locate the instability point we performed a linear extrapolation of the behavior of the smallest eigenvalue.[15] We could perform the extrapolation procedure for both branches of the spinodal line, i.e., $x<x_c$ and $x>x_c$, where x_c is the critical composition. For densities and compositions too close to the critical point, HMSA soon looses its solution at temperatures far from the critical one, where the behavior of the smallest eigenvalue is not yet linear with T. For this reason, we achieved the localization of the critical point by interpolating the two disjointed branches of the spinodal line.

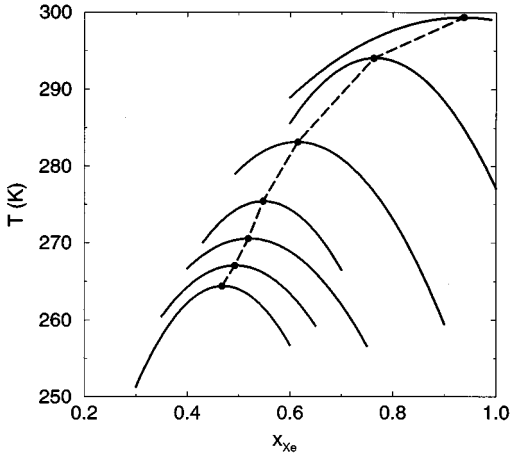

FIG. 3. Spinodal lines of Ne–Xe mixtures in the (x,T) plane. The broken line is the CPL. From top to bottom: $n=5.96\times10^{21}$, 7.01×10^{21}, 8.41×10^{21}, 9.81×10^{21}, 1.05×10^{22}, 1.12×10^{22}, 1.26×10^{22} atoms/cm^3. Interaction parameters from set 2 of Table I.

As a summary of all this procedure, we show, in Fig. 3, the spinodal lines and the line of critical points obtained by using the interaction parameters of Table I (set 2) corresponding to Ne–Xe mixtures. The plot is done in the (x,T) plane and for different values of the density.

In addition to the vanishing eigenvalue, let say λ_1, we also determined the associated eigenvector $\mathbf{X}_1(k=0)$. It gives the linear combination $(\delta\overline{n}_1(k=0))$ of composition $(\delta n^C(k=0))$ and density $(\delta n^N(k=0))$ fluctuations, [see Eq. (13)], which becomes instable and drives the transition. A measure of the relative weight of $\delta n^C(k=0)$ and $\delta n^N(k=0)$ is given, in the $(\delta n^C,\delta n^N)$ plane, by the angle α between the axis δn^C and the direction of $\mathbf{X}_1(k=0)$. The values of α can be obtained along all the spinodal line from the relation

$$\alpha=\arctan\left(\frac{X_{11}(k=0)}{X_{12}(k=0)}\right). \tag{29}$$

From Eqs. (12) and (13) we see that for $\alpha=\pm90°$ the transition mechanism is of a pure condensation/evaporation (C/E) type, while for $\alpha=0°$ we have a pure mixing–demixing (M/D) transition. However, in most cases, the angle α is in between these two values, and the transition is of combined type, since both the chemical and the mechanical stability are violated.[6]

V. THE CRITICAL LINES OF NE–XE AND HE–XE MIXTURES

As noted at the end of Sec. III, a task, which still remains unclear in the modeling of realistic fluid mixtures through the use of LJ potentials, is the choice of the parameters ϵ_{12} and σ_{12} for the mixed interaction. And such interaction parameters strongly affect the location of the spinodal lines and hence of the critical points. Then, to systematically

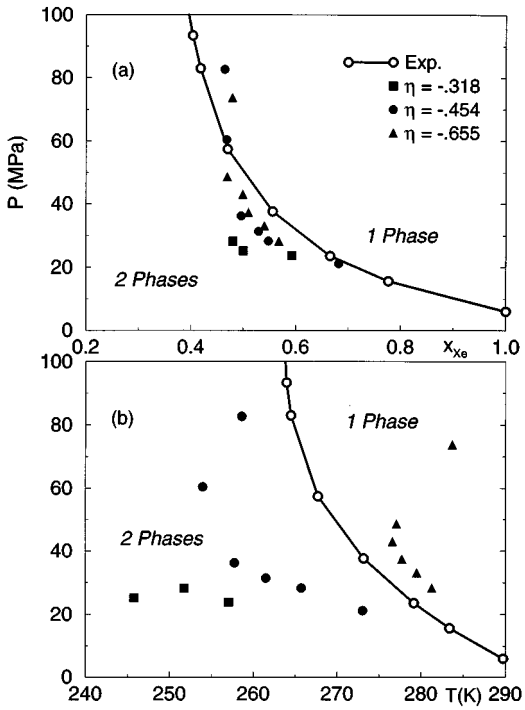

FIG. 4. Critical lines of Ne–Xe mixtures in (a) (x,P) plane and (b) (T,P) plane. The line with empty symbols are experimental data from Ref. 7. The full symbols are the results from the present theory. Interaction parameters from set 1 of Table I. For other parameters, see the text.

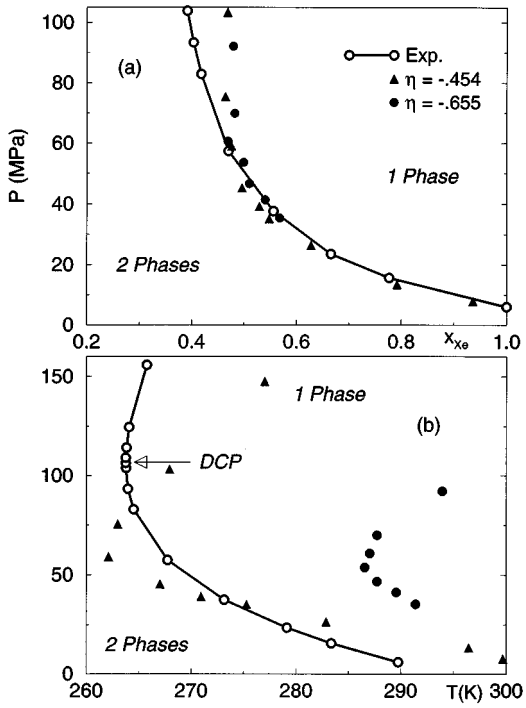

FIG. 5. Critical lines of Ne–Xe mixtures in (a) (x,P) plane and (b) (T,P) plane. The line with empty symbols are experimental data from Ref. 7. The full symbols are the results from the present theory. Interaction parameters from set 2 of Table I. For other parameters, see the text.

check the effects of different values of ϵ_{12} and σ_{12}, we introduce two parameters, η and ξ, which measure the deviation from the LB rule according to

$$\epsilon_{12}=(1+\eta)\epsilon_{12}^{\mathrm{LB}},$$

$$\sigma_{12}=(1+\xi)\sigma_{12}^{\mathrm{LB}}.$$

We performed several calculations for different values of η and ξ, and here we only present those results which indicate more clearly the trends of the critical behavior, and which are closer to the experiments. We found that changing the value of η influences the behavior of the CPL more than changing ξ. For this reason we show the results obtained by fixing ξ to the value used in Ref. 7, $\xi=0.101$, and by using a variable η. Although the critical point values are affected by numerical errors, which are generated by the interpolation between the two branches of the CPL, we prefer to show the results as they come out from the calculations, without any smoothing.

In Figs. 4(a) and 4(b) we show the critical lines in the (T,P) and (x,P) planes. The results are obtained by using set 1 for the Xe–Xe interaction parameters, and different values for the parameter η. It is evident that η must be chosen negative, and this implies a lower value of ε_{12} with respect to the LB rule. From Fig. 4(b) we see that the (T,P) representation of the critical line gives a more severe test of the theory. In this plane, the results for $\eta=-0.454$ and $\eta=-0.655$ somehow ''bracket'' the experimental data. We also see that the curve corresponding to the less negative η is strongly deviating from the realistic behavior, showing that the LB rule is completely inadequate. In the (x,P) plane the theoretical results are closer to the experimental data, but still the less negative η gives the worst results.

A better agreement with the experiments is obtained by using, for the Xe–Xe interaction, the parameters labeled as set 2 in Table I. The results are shown in Figs. 5(a) and 5(b). For $\eta=-0.454$ we get the best agreement with the experimental data, at least in the lower pressure part of the CPL. It is important to note that the ''second-type'' behavior of the CPL in the (T,P) plane is qualitatively reproduced by the theory, although the agreement is only semi-quantitative.

More simple theoretical approaches give analogous results (for short reviews see Schneider[2] and Deerenberg, Schouten, and Trappeniers[7]), but the theory outlined in this work has more predictive power. As it will be clear, it allows an understanding of the microscopic phenomena which drive the phase transition, a characterization of the transition which is generated by crossing the CPL, and the prediction of changes in the partial molar volumes, which could be experimentally measured.

To these purposes we show, in Fig. 6(b), an histogram with the values of the angle α, which have to be associated with the CPL of Fig. 6(a). In correspondence with the critical point of the pure Xe [not included in Fig. 6(a)], the angle $\alpha=90°$ and the transition is of a pure C/E type. As we move along the CPL by starting from the lowest critical pressure (which also corresponds to a continuous decrease of x_{Xe}), the angle α decreases, and becomes $\alpha=0°$ at the double critical

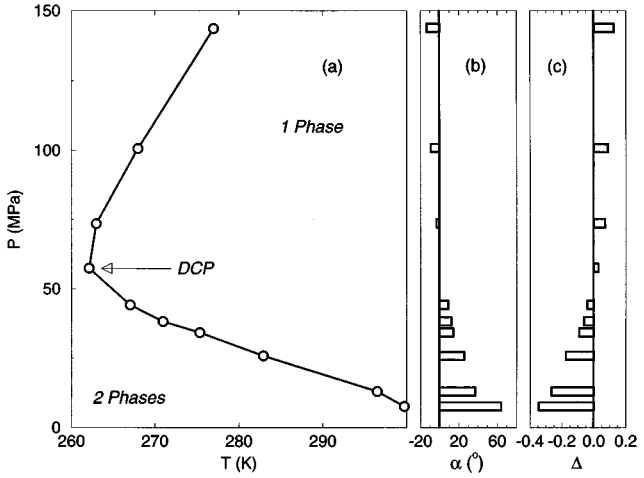

FIG. 6. (a) Theory results for the CPL of Ne–Xe mixtures. Interaction parameters from set 2 of Table I, and $\eta=-0.454$, $\xi=0.101$. (b) Values of α corresponding to the circles in (a). (c) Values of Δ corresponding to the circles in (a).

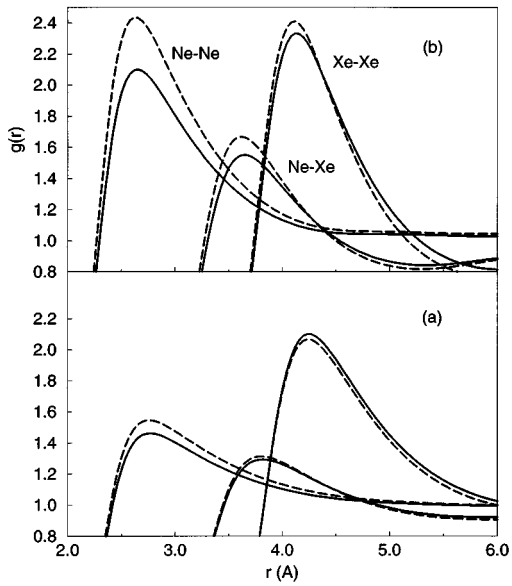

FIG. 7. Pair distribution functions of Ne–Xe mixtures. Broken lines: $x_{\mathrm{Xe}}=0.55$; continuous lines: $x_{\mathrm{Xe}}=0.45$. (a) $n=8.76\times10^{21}$ atoms/cm^3; (b) $n=1.75\times10^{22}$ atoms/cm^3. Interaction parameters from set 2 of Table I and $T=299$ K, $n=8.76\times10^{21}$, $\eta=-0.454$, $\xi=0.101$.

point. This mean that for $P\leqslant P^{\mathrm{DCP}}$, the transition mechanism smoothly changes from a pure C/E type to a pure M/D type, passing through a variety of transitions simultaneously characterized by both C/E and M/D. For $P>P^{\mathrm{DCP}}$, the angle α becomes negative, and the transitions are again of a mixed type.

To understand these results from a microscopic point of view, we have to determine the fluctuations which diverge at the instability points and which, then, drive the transition. This can be done by analyzing Eqs. (29) and (13), together with the definitions of δn^N and δn^C given in Eqs. (9) and (10). For $\alpha=90°$ there is a divergence in the number density fluctuations. For $0°<\alpha<90°$ the divergent fluctuations are a combination of δn^N and δn^C, in which both fluctuations have the same sign. For $\alpha<0°$, we still have a combination of δn^N and δn^C but, this time, with a different sign.

If in the above-mentioned equations the sub-index 1 identify Xe and 2 Ne, we can conclude the following. On the CPL and for $P<P^{\mathrm{DCP}}$ $(0°<\alpha<90°)$, the macroscopic regions of high density (positive fluctuations of δn^N), and which correspond to a new incoming phase, are more rich, with respect to their 1-phase value, of Xe particles (positive fluctuations of δn^C). At the same time, the macroscopic regions of low density (the other new phase), are more rich in Ne particles. When, instead, we are on the CPL and $P>P^{\mathrm{DCP}}$, the new incoming phase at high density are more rich, always with respect to its 1-phase value, in Ne particles, while the regions at low density are richer in Xe particles. Then when we move along the CPL and we cross the P^{DCP} or, which is the same, when we cross the corresponding $x_{\mathrm{Xe}}^{\mathrm{DCP}}$, there is a drastic change in the behavior of the systems, and at the DCP the transition is a pure M/D.

These observations are confirmed by the behavior of the dilatation factor, Δ, introduced in Eq. (11) and calculated from the ratio of Eqs. (7) and (8)

$$\Delta=-\frac{1}{(x_1x_2)^{1/2}}\frac{S_{NC}(k\to0)}{S_{CC}(k\to0)}\propto-\frac{\langle\delta n^N_{k\to0}\delta n^C_{-k\to0}\rangle}{\langle\delta n^C_{k\to0}\delta n^C_{-k\to0}\rangle},$$

the results of which are shown in Fig. 6(c).

When $\Delta\neq0$, a coupling between the density and composition fluctuations switches on. Such a coupling is absent whenever there is a pure phase transition mechanism, like at the DCP or at the critical point of pure Xe. When $P<P^{\mathrm{DCP}}$, we have $\Delta<0$ and negative (or positive) fluctuations in the composition which correspond, as we saw, to a local increase of Ne particles (or of Xe particles), are coupled with negative (or positive) fluctuations in the density which, in turns, correspond to a local decrease (or increase) of the density. These considerations are exactly the same made for the case of Fig. 6(b) with $\alpha>0$. Analogously, the conclusions reached for $\alpha<0$ apply to the case in which $\Delta>0$. Moreover, Δ being a difference of macroscopic quantities, it can be experimentally measured allowing a direct check of the results of Fig. 6(c).

Figures 7(a) and 7(b) show the partial pair distribution functions, $g_{\alpha\beta}(r)$, for cases, respectively, with $\alpha>0$, $\Delta<0$ and below the P^{DCP} and for cases above P^{DCP} $(\alpha<0,\ \Delta>0)$. The broken lines refer to $x_{\mathrm{Xe}}=0.55$, while the continuous ones to the smaller fraction $x_{\mathrm{Xe}}=0.45$. Also at the level of the $g_{\alpha\beta}(r)$, the systems show a qualitative different behavior depending on which side of the P^{DCP} they are. In particular, the number of Xe particles in the first coordination shell of $g_{\mathrm{Xe,Xe}}(r)$ increases in passing from $x_{\mathrm{Xe}}=0.55$ to $x_{\mathrm{Xe}}=0.45$ when $P<P^{\mathrm{DCP}}$ [Fig. 7(a)], while it is reduced for the same change of x_{Xe} when $P>P^{\mathrm{DCP}}$ [Fig. 7(b)].

The behavior of the CPL of He–Xe mixtures is reported in Fig. 8. For these mixtures, it was not possible to reproduce the so-called ''first type'' behavior of the CPL in the (T,P)

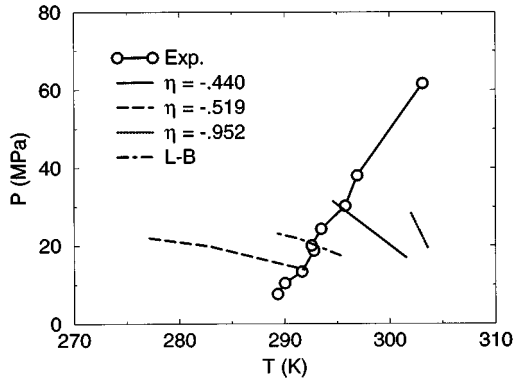

FIG. 8. Critical lines of He–Xe mixtures in (T,P) plane. The lines are the results from the present theory. Interaction parameters from set 1 of Table I. For other parameters, see the text.

plane. As observed in the figure, all the theoretical results have a wrong slope. They seem to slowly approach the right behavior for negatively large values of η, while changes of ξ do not improve the results. The ''first type'' behavior appears to be a still challenging and open problem in this kind of statistical mechanics approach.

VI. CONCLUSIONS

In order to achieve a microscopic interpretation of the gas–gas transition of binary mixtures of rare gases, we approached the problem within the framework of the density functional expansion, which allows a detailed analysis of the type of instabilities present in the systems. For the input structure we used the HMSA closure, which shows a reasonable agreement with the measured total structure factors in the single phase region. After calculating the spinodal curve for different values of the macroscopic thermodynamical parameters, we extrapolated the critical points and obtained the line of the critical points. For the Ne–Xe mixture we get the right qualitative behavior, with a critical point line showing a double critical point. It turns out that the line is strongly dependent on the parameters of the potential. Along the CPL we follow the change of the type of transition, from pure condensation–evaporation at the critical point of Xe, to the pure demixing transition at the double critical point. We also predicted the behavior of the partial volume difference along the CPL. In particular we found that it is negative for pressure below the double critical point and positive otherwise. This behavior reflects how the density and concentration fluctuations are related.

We stress that our microscopic approach, even if it is not refined enough to find a quantitative agreement, gives some understanding of the phase transition mechanism and allows predictions which could be checked by experiments. There are of course still a number of open problems. We recall that we could not reach any agreement with the first type behavior of the He–Xe mixtures, in spite of the reasonable results obtained for the structure. Even in the case of Ne–Xe it remains the problem of the best choice for the parameters of the potential, which is also common to theoretical and computer simulation approaches. We showed that these parameters are far from the Lorentz–Berthelot rule, and strongly nonadditive contributions must be taken into account. A more systematic study of different types of potentials, and of combining rules for the mixed interaction is necessary. A different behavior of the radial distribution functions has been found above and below the DCP. It has to be determined whether this is due to changes in the effective atomic forces across the DCP. On the other hand, it would be also important to compare the results obtained from the integral equation approximation with the computer simulation. This is part of the future work that we intend to carry on.

ACKNOWLEDGMENTS

We thank Professor F. Forstmann for discussions. One of us (M.R.) also thanks Professor F. P. Ricci and Professor M. Nardone for discussions and suggestions. Part of this work has been carried out with the financial support of the ''Regione Autonoma della Sardegna,'' and of the HCM network ''Colloid Physics.'' Finally, we thank Dr. P. Postorino, who made available data for the total structure factor of Ne–Xe prior to publication.

[1] J. D. van der Waals, Zittensversl. K. Akad. Wet. Amst. **1894**, 133.
[2] G. M. Schneider, in *Advances in Chemical Physics*, edited by I. Prigogine and S. A. Rice **17**, 1 (1970).
[3] J. A. Schouten, Phys. Rep. **172**, 33 (1989).
[4] *Supercritical Fluids*, edited by E. Kiran and J. M. H. Levelt Sengers (Kluwer Academic, Dordrecht, 1994).
[5] G. Malescio, J. Chem. Phys. **95**, 1202 (1991).
[6] A. Parola and L. Reatto, Phys. Rev. A **44**, 6600 (1991).
[7] A. Deerenberg, J. A. Schouten, and N. J. Trappeniers, Physica A **101**, 459 (1980).
[8] A. Z. Panagiotopoulos, Int. J. Thermophys. **10**, 447 (1989).
[9] M. R. Stapleton and A. Z. Panagiotopoulos, J. Chem. Phys. **92**, 1285 (1990).
[10] A. Z. Panagiotopoulos, Mol. Simul. **9**, 1 (1992).
[11] X. S. Chen and F. Forstmann, J. Chem. Phys. **97**, 3696 (1992).
[12] M. C. Bellisent-Funel, U. Bountempo, A. Filabozzi, M. Nardone, and F. P. Ricci, Phys. Rev. A **46**, 1002 (1992).
[13] A. Filabozzi, M. Nardone, P. Postorino, and F. P. Ricci (private communication).
[14] G. Zerah and J. P. Hansen, J. Chem. Phys. **84**, 2336 (1986).
[15] J. Bergenholtz, P. Wu, N. J. Wagner, and B. D'Aguanno, Mol. Phys. **87**, 331 (1996).
[16] H. B. Callen, *Thermodynamics* (Wiley, New York, 1960).
[17] J. G. Kirkwood and F. P. Buff, J. Chem. Phys. **19**, 774 (1951).
[18] A. B. Bhatia and D. E. Thornton, Phys. Rev. B **2**, 3004 (1970).
[19] D. Gazzillo, Mol. Phys. **83**, 1171 (1994).
[20] D. Gazzillo, Mol. Phys. **84**, 303 (1995).
[21] F. J. Rogers and D. A. Young, Phys. Rev. A **30**, 999 (1984).
[22] J. D. Weeks, D. Chandler, and H. C. Andersen, J. Chem. Phys. **54**, 5237 (1971).
[23] J. C. Ng, J. Chem. Phys. **61**, 2680 (1974).